Progress report for 2007 SCEC Proposal

Title of Project:

Continued study - Constraints on pulverization conditions from damage pattern of sedimentary rocks along the San Andreas Fault in the Mojave.

Name of PI:

Yehuda Ben-Zion
Department of Geological Sciences
University of Southern California

With graduate student Ory Dor
Department of Geological Sciences
University of Southern California

***Proposal Categories*:**
Data Gathering and Products
Integration and Theory

Science objectives:
A7, A8, A9

Summary:
This report summarizes our 2007 SCEC funded research on the properties of damaged and pulverized sandstones along the San Andreas Fault (SAF) in the Mojave Desert. The work addresses topics that required further investigation following our previous SCEC funded studies (Dor et al. EPSL, PAGEOPH 2006) regarding the depth extent of pulverization and the mechanism of rock pulverization during seismic rupture. Toward this we examined the extent and type of damage in sedimentary rocks that were not buried deeply while being displaced along the SAF. In last year's report we presented our research approach and the methodologies we used together with initial results we obtained. Here we present a summery of the results from 2007 (Dor, PhD thesis, USC), showing that pulverization in sandstones of the Juniper Hills formation in the Mojave is similar to pulverization of crystalline rocks from the same fault section. We found that damage in this sandstone has a clear spatial association with the trace of the SAF. Assuming that the SAF slipped seismically during the displacement of the Juniper Hills sandstone, which was never buried more than few tens of meters, the results imply that dynamic generation of damage can occur close to the surface of the Earth. Initial fracture orientation analysis suggests that this type of damage may be the result of stress concentrations due to seismic slip on frictional wavy fault and possibly due to fault-normal vibrations and an opening mode associated with the rupture tip stress field.

Geological setting and methodologies

The late Pliocene-early Pleistocene Juniper Hills Formation (hereafter JHF) consists of material derived from the Punchbowl formation and several other clasts types not found in older sedimentary rocks. It is a tectonostratigraphic unit deposited in basins parallel to the SAF and its subsidiary faults in the area. The entire sedimentary and deformation history of this formation is therefore associated with activity of fault strands in the central Mojave section of the SAF system. Distinctive JHF unites with unique clasts content are offset 13 to 16 km by the Northern Nadeau fault and 19 to 21 km by the SAF in and adjacent to our study area. Various evidence exist that the JHF was never buried deeply.

Figure 1 shows the distribution of some of the JHF bodies southwest of the SAF with our sampling locations. Our qualitative and quantitative description is based on 13 oriented samples of the JHF member TQjh collected at 7 stations along a fault-normal traverse. We compare this description to observations from 3 samples of the Hungry Valley formation collected at distances of 125 to 3380 m from the SAF in the northwest portion of the Mojave Desert and in Ridge Basin.

Image analysis: We mapped the original grain boundaries of 170-230 individual grains for each thin section. The digitized grain map was analyzed in the image analysis software "Image J" to yield a grain map and an associated data set. We divided the grain population into 4 size bins from which we chose 12 grains for detailed analysis.

Each of the selected grains was photographed under reflected light in an X100 magnification. We used this image to generate two products: the first was a grayscale image of the grain itself masked from the background, and the second was an image of the exact trace of the grain boundary, which was used as a reference for the original "intact" grain. The image of the masked grain was transformed into a bitmap (binary) mode using 50% threshold value and then inverted. The two images were then analyzed in Image J for their total perimeter length, and we calculated the Factor of Increase in

Perimeter Length (FIPL) by dividing the total perimeter lenth of the “damaged” grain in that of the “intact” grain. The FIPL for the entire sample is an area-weighted average of the FIPL of all the grains that were analyzed in that sample (in calculating the average, grains were given weight according to their original area).

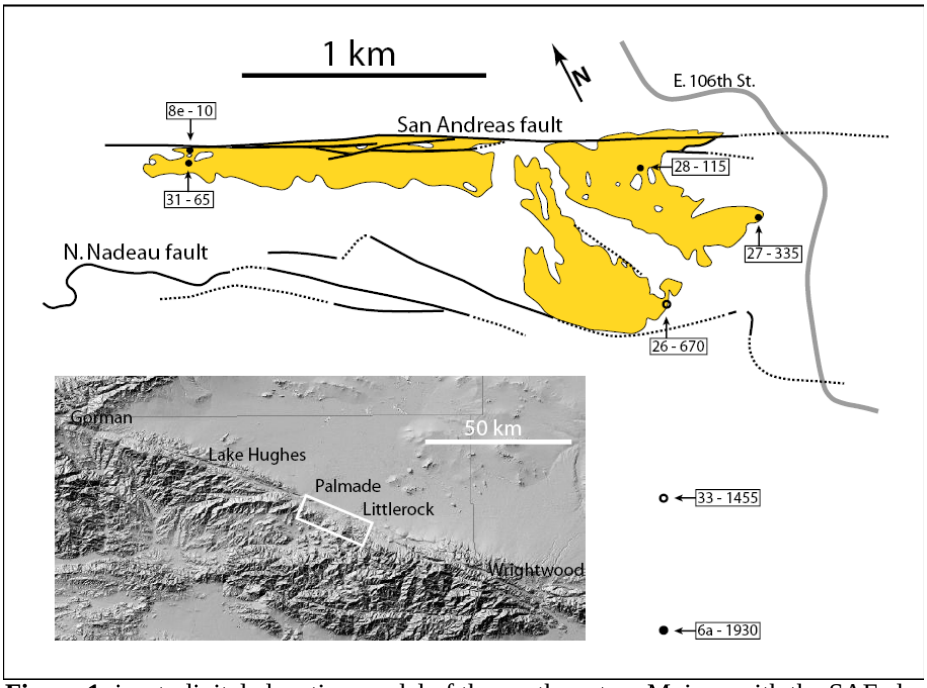

Figure 1: inset: digital elevation model of the southwestern Mojave with the SAF clearly seen as a linear scarp separating the San Gabriel Mountains from the Mojave Desert floor. The sampling area is marked (includes the area in the larger map + location of samples 6a and 33). The larger map (after Barrows et al., 1985) shows the distribution of some of the JHF bodies in the area with the location of our sampling points. For samples 6a and 33 we show only the distance to the fault, not their geographic location. Note that the JHF here is bounded by the SAF and the N. Nadeau fault.

Fracture orientation measurements: The following are types of microfractures observed and measured for orientation in our samples, distinguished according to their relations to grain size and to their hierarchical internal arrangement within and with respect to the grain:

Type I: Fractures that cut an entire grain. They are frequently parallel to each other, dissecting the grain or part of it to elongated, columnar fragments.

Type II: Fractures that cut at least half of the grain’s width in the direction of the fracture, and terminate within a grain. Some of them taper into the grain while others connect fractures to other fractures or to grain boundaries.

Type III: Considerably shorter than the grains average axis length. Those are usually connecting fractures that terminate against type I or II fractures. They often cut elongated columnar fragments into rectangular or otherwise angular fragments, creating webs in crisscrossing relationship (e.g. category II fractures of Laubach, 1997,).

Type IV: Fluid inclusion plains: those are shown as linear traces of bubbles, marking the location of healed (or sealed) fractures (e.g. Tuttle, 1949).

Observations

1. Common damage features present in all/most samples (Figure 2):

a. Heavily fragmented grains: the grain is fractured into many fragments significantly smaller than the grain itself with large increase in the total perimeter length. Frequently the fragments have high aspect ratio (high circularity values)

b. Partially fractured grains: part of the grain is fragmented and part of it is intact. Some partially fractured grains have one or just few long fractures.

c. Deformed mica crystals: mica crystals kinked and squeezed due to a displacement of another, more rigid grain. Suggestive of operation of compressional forces.

d. Impingement (Hertzian) fractures: fractures that appear to emanate from grain boundaries at a high angle. If more than one fracture is present, the fractures tend to be arranged in a parallel, radiating or cone geometries radiating from the grain-grain contact. Those fractures tend to form elongated columnar fragments that are often divided into shorter fragments by intermediate and short connecting fractures (possibly due to bending of the elongated fractures). Those long, intermediate and short fractures correspond to fracture types II, III and IV described above, respectively. These types of fractures were produced in the short term compaction creep experiments of Chester et al. (2004).

In general, damage is highly heterogeneous in all samples, with some grains fragmented down to the micron scale while others remaining intact. Visually, fault-parallel and other shear components are apparently absent at all scales: sedimentary fabrics are intact and even the most fractured grains, with few exceptions, preserve their original outline, with the fragments appearing to fit together in a hierarchical fashion.

2. FIPL measurements:

Accuracy of the method: The statistical significance of the method was tested on a large population of analyzed grains from sample 8E-b. This sample was taken 10 m from the fault and is highly variable in its grain sizes and their fracture content. We mapped 186 grains on the thin section and analyzed 104 of them. The area-weighted average FIPL for all the 104 grains is 8.14 and the area-weighted standard deviation is 5.34 (Table 1). 10 sets of 40 grains were chosen randomly from the 104 grains population. Their area-weighted average FIPL and area-weighted standard deviations are presented in Table 1. We performed t-test in order to verify that the sets chosen are indeed representative of the larger population. None of the sets is statistically different from the parent population (the *P* values of all of them is larger than 0.05, and for some of them it is closer to 1; all the sets pass Shapiro-Wilk and Shapiro-Francia W normality tests with over 95% probability), suggesting that the sampling method captures the properties of the entire grain population (assuming that the 104 grains are representative of the grains in the sample).

Table 1: Area-weighted average FIPL and standard deviation for the 104 grains population analyzed from sample 8E-b and for each of the 40-grains sets chosen from this population. T-test results show no statistical difference between each of the sets and the entire population.

40 grains Set	**1**	**2**	**3**	**4**	**5**	**6**	**7**	**8**	**9**	**10**	**Aver-age**	***all 104 grains***
FIPL	7.40	8.06	7.09	6.10	8.72	8.40	7.99	7.15	8.92	7.29	7.71	8.14
A. weighted STDV	4.45	5.84	4.35	3.48	6.01	5.25	5.03	4.37	5.02	4.18	4.8	*5.34*
t-test *P* value	0.8	0.92	0.86	0.86	0.82	0.95	0.72	0.28	0.42	0.54		

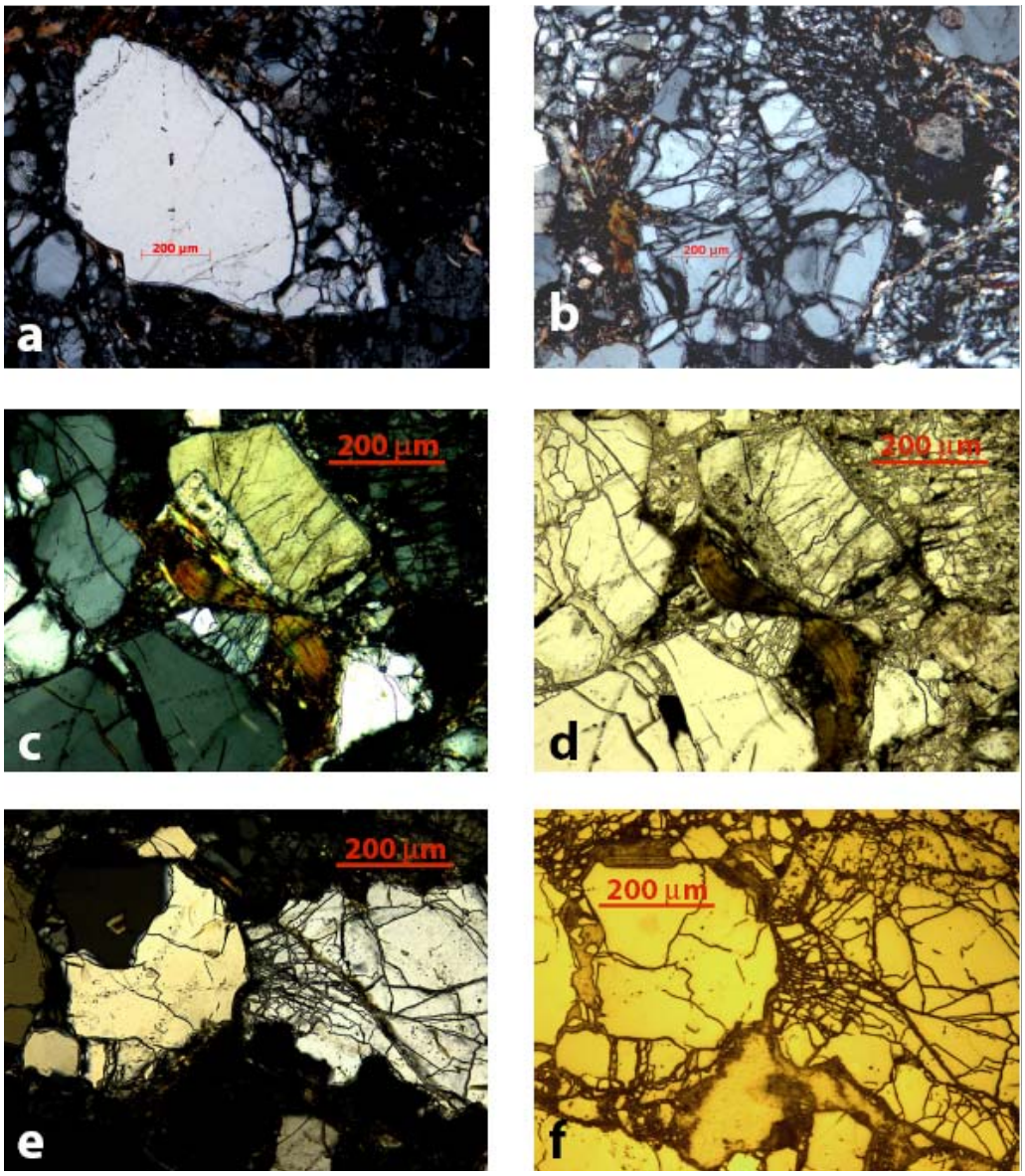

Figure 2: microscale damage features: a. Partially fractured grain. b. Heavily fractured grain. Note the three columns of fragments: may be caused by impingement, like in (e, f). c, d. Cross polarized (c) and transmitted (d) photos of bended and sheared mice grain, in this case clearly due to an impingement between the two grains in contact: note the fractures radiating from the grain on the left. e, f. Cross polarized (e) and reflected (f) photos of fractures radiating in a Hertzian pattern from a contact zone between two grains.

Results of FIPL measurements along the traverse: Our measurements are summarized in Table 2, confirming the pattern observed by qualitative examination of the thin sections. The FIPL is highest in the sample taken 10 m from the fault and is still high in the sample taken 65 m from the fault. Farther away from the fault the FIPL decreases but there is apparently no strong drop in its values. A t-test shows that the samples taken at 10, 65 and 115 m from the fault are statistically different from each other, while the samples taken at 115, 335 and 1930 m from the fault are statistically indistinguishable from each other in their FIPL values distribution. All sample results passed Shapiro-Wilk

and Shapiro-Francia W normality tests with over 95% probability. These results suggest that the damage gradient is significant in the ~100 m distance from the fault, after which the damage gradient becomes insignificant.

Table 2: summary of measurements done on the JHF samples.

Sample	8E-b	31	28	27	6a
distance from fault	10	65	115	335	1930
FIPL	***8.14***	***5.21***	***2.42***	***3.81***	***1.53***
Thin section inclination	28	70	80	46	83
t-test *P* value[1]		0.00	0.00	0.4	0.38

1. For each sample with respect to the next sample closer to the fault.

From the sample taken 10 m from the fault we made three thin sections, one of them been vertical in its real-world orientation. Since the two inclined thin sections contained many more fractures than the vertical one, we concluded that at least at this location, fractures are leaning to verticality.

Table 3: Rose diagrams showing the distribution of orientations for the various fracture types from samples 8E-b and 31 with corresponding statistics. Red line marks the orientation of the SAF in the area.

Type	**Sample 8E-b, 10 m SW of SAF**	**Sample 31, 65 m SW of SAF**
I	No. of Data = 40 Mean dir'n = 042-222 95% Confidence = ±22°	No. of Data = 51 Mean dir'n = 115-295 95% Confidence = ±54°
I	No. of Data = 95 Mean dir'n = 054-234 95% Confidence = ±26°	No. of Data = 90 Mean dir'n = 139-319 95% Confidence = ±44°
II	No. of Data = 428 Mean dir'n = 027-207 95% Confidence = ±16°	No. of Data = 500 Mean dir'n = 145-325 95% Confidence = ±53°
I	No. of Data = 84 Mean dir'n = 137-317 95% Confidence = ±90°	No. of Data = 41 Mean dir'n = 177-357 95% Confidence = ±90°

3. Orientation of microfractures:

The results of the fracture orientation measurements are displayed in Table 3. Despite the scattering in strike direction, the two samples show preferred orientation of fracture types I, II and III that is distinctly different between the samples. Fracture type IV (fluid inclusion plains) show 95% confidence interval of 90 degrees, i.e. no preferred orientation in both samples. Those fractures are likely inherited from the source rock and were not formed in the process that created the other fracture types.

Discussion

1. Structure of the damage zone (on the southwest side of the SAF): the results presented in Table 2 suggest that the width of the damage zone is of the order of 100 m. This length scale for the (half) width of the damage zone was observed (including in the distribution of microscale damage) for many other fault zones (e.g. Wilson et al., 2003). Furthermore, the length scale of ~100 m is also the average width of the crystalline pulverized rocks layer which is slightly wider in our working area (Dor et al., 2006a). We found similar features for the Hungry Valley formation from the northwest portion of the SAF in the Mojave, with the damage there been more intense and the damage zone wider.

2. Mechanical interpretation of damage fabric: The observation of grains shattered in-situ, preserving their original outlines is overwhelmingly systematic and common to both crystalline and sedimentary rocks spatially associated with the SAF. Our observations are consistent with failure of grains in a compressional field. First, we observe numerous damage elements typical of grain contact pressure, in particular impingement (Hertzian) fractures, and second, mapping of several hundreds of fractures in two samples show that open fractures, which are likely associated with current or recent fault activity, have a preferred orientation that is especially strong near the fault. We inferred that the fractures near the fault are mostly sub-vertical.

3. Implications of results for dynamic rock failure: The JHF was deposited in between and displaced by strands of the SAF system that are currently or recently active, and therefore its entire damage history is most likely related to the current faulting regime. We therefore conclude that damage in elevated levels within ~100 m from the active trace of the SAF is the product of fault activity, i.e. large SAF earthquake ruptures. Although some grains can survive transportation while they are partially fractured, the intense fracturing we see with open fractures that frequently cut the entire width of the grain suggest that fracturing occurred mostly in-situ and was not inherited from the source rock. The clear preferred orientation of the fractures is independent evidence that fracturing is post-depositional.

The JHF was never deeply buried and therefore this damage was generated shallow in the crust, probably at depths of several hundreds of meters and possibly within meters from the surface of the Earth. This inference is supported by the lack sealing or healing of the fractures. For the fractures to remain open, ground water filtration and temperatures mast have been minimal. Fluid inclusion planes (healed fractures), that form a small minority in the fracture population, are cut by open fractures, have no preferred orientation, and are therefore likely inherited from the source rock.

The nature of damage in pulverized crystalline rocks spatially associated with the trace of the SAF (Dor et al., 2006a), although not studied systematically so far in the microscale, appears to be qualitatively similar to that observed in our study. This may suggest that pulverization can occur very close to the surface of the earth, in agreement with previous inferences about minimal exhumation in the area and with theoretical considerations.

The anisotropy of the damage fabric and the abundance of damage elements associated with pressure show that absolute tension was probably not the primary mechanism responsible for the failure of the JHF rocks. The microfractures in sample 8E-b are preferably orientated normal to the SAF. Chester and Chester (2000) presented a mechanical modeling of stress and deformation in the vicinity of a wavy frictional

surface and showed that due to the juxtaposition of geometric irregularities and under loading conditions relevant for the SAF (i.e. with relatively high angle between the maximum far-field compressive stress and the fault), the maximum near-field principal compressive stress during cyclic loading associated with slip events is oriented nearly normal to the fault surface. In such conditions, fractures normal to the fault surface may form throughout the damage zone of the fault.

Fault opening and significant reduction of normal stress are expected to produce a change in the orientation of stresses as a function of distance from the fault. This may lead to a variability in the preferred orientation of microfractures within the damage zone that reflect changes from the background stress to near-zero transient shear stress on the fault. The change in preferred orientation of microfractures between the samples at 10 and 65 m from the fault is therefore compatible with strong dynamic reduction of normal stress or fault opening.

4. Summary: The distribution of damage we observe delineates a ~100 m wide damage zone on the southwest side of the SAF near Littlerock, California. Assuming that the SAF was seismically active since the deposition of the JHF in the late Pliocene – early Pleistocene and due to the clear spatial association that the damage has with the trace of the fault, we conclude that this damage was generated during SAF earthquakes. The exhumation history of the area, the poor consolidation state of the rock and the significant abundance of open fractures with preferred orientations within the damage zone are all compatible with generation of damage close to the surface of the Earth during seismic events.

A future study will be focused on similar types of measurements done on a denser array of samples taken along this and other traverses, with the purposes of improving the precision of the FIPL measurements and delineating more precisely the damage gradient and the variations in fracture orientations with respect to the fault. Future results will be used to infer on the actual increase in surface area due to fracturing at shallow depth, and to constrain rupture mechanism and strong ground motion in the immediate vicinity of the San Andreas and other large faults.

Publications supported by this grant

Dor, O, Y Ben-Zion, J S Chester, J Brune, T K Rockwell, Damage Characterization in Sandstones Along the Mojave Section of the San Andreas Fault With a new Method: Initial Results and Implications for the Depth and Mechanism of Dynamic Rock Fragmentation, Eos Trans. AGU, 88(52), Fall Meet. Suppl., Abstract T14A-03, 2007.

Dor O., Ben-Zion, Y., Chester, J., Rockwell, T.K., and Brune J.N., Damaged sandstones from the Mojave section of the San Andreas Fault: implications for the depth and mechanism of dynamic rock pulverization, manuscript in prep., 2008.

References

Barrows, A.G., Kahle, J.E. and Beeby, D.J. (1985). Earthquake Hazard and tectonic history of the San Andreas Fault zone, Los Angeles County, California. Open file report 85-10 LA., California Department of Conservation, Division of Mines and Geology.

Chester, F.M., Chester, J.S., (2000). Stress and deformation along wavy frictional faults. *J. Geophys. Res.* 105, 23,421–23,430.

Chester, J.S., Lenz, S.C., Chester, F.M. and Lang, R.A. (2004). Mechanisms of compaction of quartz sand at diagenetic conditions. *Earth Planet. Sci. Lett.* 220, 435-451.

Dor (2007), Symmetry properties, pulverized rocks and damage architecture in fault zones as signatures of earthquake ruptures. PhD Thesis, University of Southern California, 306 pp.

Dor, O., Ben-Zion, Y., Rockwell, T.K., and Brune J.N. (2006a). Pulverized Rocks in the Mojave section of the San Andreas FZ, *Earth Planet. Sci. Lett.* 245, 642-654. doi:10.1016/j.epsl.2006.03.034.

Dor, O., T.K. Rockwell, and Y. Ben-Zion (2006b). Geologic observations of damage asymmetry in the structure of the San Jacinto, San Andreas and Punchbowl faults in southern California: A possible indicator for preferred rupture propagation direction. *Pure Appl. Geophys.*, 163, DOI 10.1007/s00024-005-0023-9.

Laubach, S.E., 1997. A method to detect natural fracture strike in sandstones. *Am. Assoc. Petroleum Geologist Bull.* 81, 604–623.

Tuttle, O.F. (1949). Structural petrology of planes of liquid inclusions, *J. Geology*, 57, 331-356.

Wilson, J. E., Chester, J. S. & Chester, F. M. (2003). Microfracture analysis of fault growth and wear processes, Punchbowl Fault, San Andreas System, California. *J. Struct. Geol*. 25, 1855–-1873.